Visualization of the exocyst complex dynamics at the plasma membrane of *Arabidopsis thaliana*

Matyáš Fendrych[a,*], Lukáš Synek[a], Tamara Pečenková[a,b], Edita Janková Drdová[a], Juraj Sekereš[a], Riet de Rycke[c], Moritz K. Nowack[c], and Viktor Žárský[b]

[a]Institute of Experimental Botany, Academy of Sciences of the Czech Republic, 165 02 Prague 6, Czech Republic;
[b]Department of Experimental Plant Biology, Faculty of Science, Charles University, 128 44 Prague 2, Czech Republic;
[c]VIB Department of Plant Systems Biology, Ghent University, 9052 Gent, Belgium

ABSTRACT **The exocyst complex, an effector of Rho and Rab GTPases, is believed to function as an exocytotic vesicle tether at the plasma membrane before soluble *N*-ethylmaleimide–sensitive factor attachment protein receptor (SNARE) complex formation. Exocyst subunits localize to secretory-active regions of the plasma membrane, exemplified by the outer domain of *Arabidopsis* root epidermal cells. Using variable-angle epifluorescence microscopy, we visualized the dynamics of exocyst subunits at this domain. The subunits colocalized in defined foci at the plasma membrane, distinct from endocytic sites. Exocyst foci were independent of cytoskeleton, although prolonged actin disruption led to changes in exocyst localization. Exocyst foci partially overlapped with vesicles visualized by VAMP721 v-SNARE, but the majority of the foci represent sites without vesicles, as indicated by electron microscopy and drug treatments, supporting the concept of the exocyst functioning as a dynamic particle. We observed a decrease of SEC6–green fluorescent protein foci in an *exo70A1* exocyst mutant. Finally, we documented decreased VAMP721 trafficking to the plasma membrane in *exo70A1* and *exo84b* mutants. Our data support the concept that the exocyst-complex subunits dynamically dock and undock at the plasma membrane to create sites primed for vesicle tethering.**

Monitoring Editor
Patrick J. Brennwald
University of North Carolina

Received: Jul 2, 2012
Revised: Dec 17, 2012
Accepted: Dec 19, 2012

INTRODUCTION

Plant surfaces are products of secretory pathways. The final decisive step in secretion is exocytosis, resulting in the fusion of membrane vesicles with the plasma membrane (PM) and delivery of the vesicle content to the cell surface—the apoplast. All of the different "direct secretion" systems at the PM (e.g., ion transporters, cellulose synthases, and ABC transporters responsible, among others, for cell wall modifications) are brought to the PM by exocytosis. An intricate balance between exocytosis and endocytosis (i.e., membrane recycling) is the basis for proper PM system functioning (Battey *et al.*, 1999). Despite its importance, we know surprisingly little about mechanistic details of plant exocytosis.

The secretory vesicle life cycle includes its budding from the donor membrane, transport, and finally tethering and fusion with the destination membrane (Cai *et al.*, 2007). The vesicle–target membrane fusion is achieved by a coordinated action of tethering factors and soluble *N*-ethylmaleimide–sensitive factor attachment protein receptor (SNARE) proteins (Söllner *et al.*, 1993). The tethering machinery includes Rab GTPases, coiled-coil tethering proteins, and multisubunit tethering complexes. Vesicle tethering precedes the membrane fusion catalyzed by SNARE proteins by bridging the vesicle and the PM (reviewed in Bröcker *et al.*, 2010). Distinct phases of exocytic vesicle tethering and docking at the target membrane have been described in detail in animal cells, but such a resolution has not been achieved in plants, and therefore we use the term "tethering" sensu lato. The exocyst is an octameric protein complex that tethers vesicles to the PM and is composed of the SEC3, SEC5, SEC6, SEC8 SEC10, SEC15, EXO70, and EXO84 subunits in

This article was published online ahead of print in MBoC in Press (http://www.molbiolcell.org/cgi/doi/10.1091/mbc.E12-06-0492) on January 2, 2013.

*Present address: VIB Department of Plant Systems Biology, Ghent University, 9052 Gent, Belgium.

Address correspondence to: Matyáš Fendrych (fendrych@ueb.cas.cz).

Abbreviations used: PM, plasma membrane; VAEM, variable-angle epifluorescence microscopy.

animals, yeast, and plants (Heider and Munson, 2012). In yeast, the exocyst binds the vesicle via interaction of the Sec15 subunit with the vesicle-associated Sec4 Rab GTPase (Guo *et al.*, 1999b). Attachment of the exocyst to the PM is achieved by interactions with Cdc42, Rho1, and Rho3 GTPases in yeast (Robinson *et al.*, 1999; Guo *et al.*, 2001; Zhang *et al.*, 2001) and possibly via the ROP/RAC effector ICR1 in *Arabidopsis* (Lavy *et al.*, 2007). In yeast, the exocyst is further linked to the PM by direct binding of Exo70 and Sec3 subunits to phosphatidylinositol 4,5-bisphosphate (He *et al.*, 2007; Zhang *et al.*, 2008) and by interaction of Sec6 with the Sec9 t-SNARE (Sivaram *et al.*, 2005). In *Arabidopsis*, the EXO70B2 exocyst subunit interacts with the SNAP33 SNARE (Pečenková *et al.*, 2011). Organisms defective in exocyst subunits typically suffer from secretion defects (Novick *et al.*, 1980; Guo *et al.*, 1999a). *Arabidopsis* exocyst mutants are indeed defective in seed coat pectin exocytosis, pollen tube, root hair, and hypocotyl growth. In addition, the exocyst complex localizes to secretory-active PM domains in plant cells, similar to the situation in other eukaryotes (Cole *et al.*, 2005; Hála *et al.*, 2008; Žárský *et al.*, 2009; Fendrych *et al.*, 2010; Kulich *et al.*, 2010). Both facts suggest a role for the exocyst in exocytosis in plant cells.

As the action of the exocyst depends on its precise localization to the PM, the data indicate localization of the bulk of exocyst proteins to membrane domains associated with high secretion activity (Finger *et al.*, 1998; Lipschutz *et al.*, 2000; Gromley *et al.*, 2005; Fendrych *et al.*, 2010). Detailed analysis of the exocyst localization at the PM is lacking. Whereas endocytosis was characterized by visualizing the assembly of clathrin light chain and dynamin-related proteins at single endocytic sites in *Arabidopsis* (Konopka and Bednarek, 2008a; Konopka *et al.*, 2008; Fujimoto *et al.*, 2010), there is no similar framework for exocytic events. The exocyst is considered a vesicle-tethering machinery. However, when the exocyst subunits are recruited to secretory vesicles and to the PM, whether the exocyst actually colocalizes with secretory vesicles, and the dynamics of the exocyst at the PM are not known. To fill this gap, we use a combination of advanced microscopy techniques and genetic and pharmacological experiments in *Arabidopsis* plants expressing fluorescently tagged exocyst subunits and *Arabidopsis* exocyst mutants.

RESULTS

Exocyst subunits colocalize in distinct foci at the plasma membrane

In *Arabidopsis thaliana*, green fluorescent protein (GFP)–tagged exocyst subunits SEC6, SEC8, EXO70A1, and EXO84b are enriched at the outer PM of root epidermal cells and localize strongly to post-cytokinetic cell plate membranes (Figure 1A; Fendrych *et al.*, 2010). The PM signal is not homogeneous, and we occasionally observed dim spots at high magnification using the confocal laser scanning microscope (CLSM). To achieve higher spatial resolution and to separate the signal of exocyst subunits at the PM from the fluorescence of subunits in cytoplasm, we used variable-angle epifluorescence microscopy (VAEM; Konopka and Bednarek, 2008b), which enables illumination of objects in close proximity to the microscope slide. We examined roots of *Arabidopsis* seedlings expressing SEC6-GFP, GFP-SEC8, and EXO84b-GFP under the control of genomic promoters and EXO70A1-GFP under the control of the constitutive 35S promoter (Fendrych *et al.*, 2010). Functionality of the exocyst-subunit localizations is corroborated by the ability of EXO84b, EXO70A1, and SEC8 GFP-fusion proteins to complement mutations in the respective genes (Fendrych *et al.*, 2010; Kulich *et al.*, 2010). We observed localization of GFP signal into distinct foci at the PM (Figure 1B). In the meristematic zone it was sometimes difficult to distinguish individual foci, and therefore we determined the density of the foci in elongation and maturation zones (Figure 1C). Density decreased from the root meristematic zone to the maturation zone from ~1.6 to 1.3 foci/μm^2; this difference was statistically significant for the EXO84b, EXO70A1, and SEC8 subunits (analysis of variance, $\alpha = 0.05$).

To test whether exocyst subunits colocalize in the PM foci, we crossed *Arabidopsis* plants expressing GFP-tagged exocyst subunits with plants expressing monomeric red fluorescent protein (mRFP)–tagged SEC6 or EXO84b subunits. The mRFP- and GFP-labeled foci colocalized in ~37% (Figure 2, A and B). We also observed a high proportion (~50%) of only GFP-labeled foci and a small proportion (~7–17%) of only mRFP-labeled foci in all combinations (Figure 1, D and E). Probably due to silencing of the GFP-EXO70A1 transgene, we were unable to obtain any GFP-EXO70A1 and mRFP-positive plants in the progeny of the respective crosses. Patterns of endocytic events in *Arabidopsis* epidermal cells when visualized by dynamin-related proteins (DRP) and the clathrin light chain protein fusions (Konopka and Bednarek, 2008a; Konopka *et al.*, 2008) resemble that of exocyst foci. We therefore analyzed possible colocalization of DRP1C-mOrange with GFP-SEC8 and found that it was low, ~10%, similar to the colocalization of exocyst foci caused by a random overlap (Figure 1, D and E, and Supplemental Figure S1A).

Taken together, the results show exocyst subunits colocalized in the PM foci that were clearly distinct from endocytic sites marked by DRP1C.

Dynamics of exocyst foci and dependence on the cytoskeleton

The exocyst-labeled foci displayed limited spatial motility that preceded or followed dwelling of the foci at the PM. The signal usually appeared and remained localized to an identical site and vanished eventually (Figure 2A and Supplemental Videos S1 and S2). To monitor the foci behavior in time, we used kymographic representations of the time series, where the bona fide exocytic events appear as a straight line (Figure 2A). The signal intensity typically increased after its appearance, and later decreased before its disappearance. There was no prevailing pattern of signal maxima or minima during the event. Exocyst subunits colocalized in the foci during the whole event (Figure 2B).

The median lifetime (represented by the length of straight lines in kymographs) of exocyst foci in cells of elongation and root hair zones as determined from kymographs was 9.4, 13.3, 9.3, and 11.8 s for SEC6, SEC8, EXO70A1, and EXO84b, respectively. The lifetime distribution was similar for all exocyst subunits tested (Figure 2D).

To assess the exocyst turnover at the PM and to measure the turnover of the bulk of exocyst subunits, we performed fluorescence recovery after photobleaching (FRAP) experiments using CLSM. We infer from the FRAP curves that the mobile fraction of exocyst subunits is high, representing ~90% (Figure 2C). The fluorescence recovery half-time was 23.4 ± 8.9, 19.9 ± 9.6, 38.1 ± 17.3, and 36.0 ± 6.5 s for the SEC6, SEC8, EXO70A1, and EXO84b subunit, respectively (± represents SD). The FRAP experiments show that the exocyst subunits cycle between cytoplasm and PM approximately on the order of tens of seconds for all four subunits studied. The FRAP values were higher than the foci lifetimes, which can be caused by the fact that the laser also bleaches populations of foci in adjacent focal planes.

The exocyst is known to be sensitive to actin disruption in yeast cells (Boyd *et al.*, 2004). First, we analyzed the possible colocalization of the exocyst (represented by EXO84b-GFP) with the actin marker Lifeact-mRFP (Riedl *et al.*, 2008) and found no significant

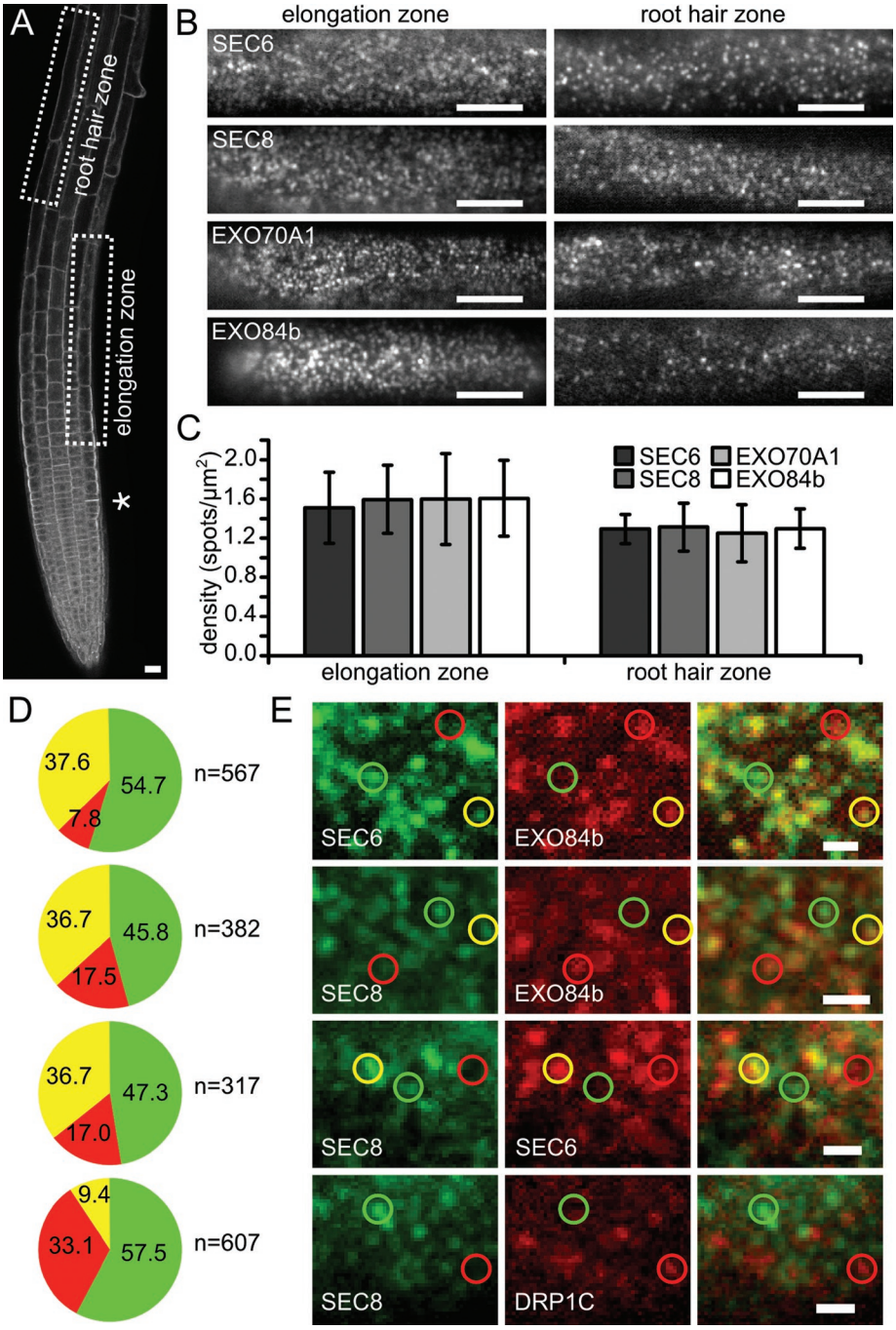

FIGURE 1: Exocyst subunits colocalize in distinct foci at the plasma membrane. (A) CLSM section of *Arabidopsis* root expressing EXO84b-GFP. The signal decorates outer epidermal PM. In recently divided cells, the exocyst is focused on the maturing cell walls (asterisk). (B) Exocyst subunits form distinct foci at the PM when observed by VAEM. Foci appearance is shown in the PM of outer epidermal root cells in elongation (left) and root hair zones (right). Scale bars, 10 μm. (C) Exocyst foci density in root epidermal cells; $n \geq 10$ cells for each column; error bars, SDs. (D) Quantification (%) of the exocyst subunits and DRP1C colocalizations in *Arabidopsis* root epidermal cells. Pairs indicated in E were evaluated. Green, red, and yellow colors represent GFP only, mRFP only, and their colocalization, respectively. (E) Localization of SEC6, SEC8, and EXO84b exocyst subunits. Green, red, and yellow circles denote GFP-only, mRFP-only, and GFP- and mRFP-positive foci, respectively. Scale bars, 1 μm.

colocalization (Figure 3A). Second, upon 10 min of actin disruption by latrunculin B (latB), the exocyst appearance remained unaffected. After 1-h latB treatment, exocyst foci were still present; however, in some cells the foci aggregated into clusters (Figure 3C). The effect was more obvious when using the CLSM, as the latB effect was pronounced in the epidermal cells below the lateral root cap, and these cells are inaccessible for VAEM. The exocyst aggregated into cell corners and formed clusters of intensive signal in epidermal cells in the elongation zone (Figure 3E).

The exocyst is known to associate with microtubules (MT) in animals (Vega and Hsu, 2001; Wang *et al.*, 2004). However, we did not observe any significant colocalization when EXO84b-mRFP was expressed with the MAP4-GFP MT marker (Marc *et al.*, 1998; Figure 3B). The exocyst appearance at the PM remained unchanged after either 10-min or 1-h MT disruption by amiprophos methyl (Figure 3, B and D).

We further examined possible cytoskeletal drug effect on the EXO84b-GFP turnover at the PM using FRAP. Whereas 1-h MT disruption had no obvious effect, 1-h actin disruption led to a significant retardation of exocyst recruitment to the PM (Figure 3G).

These data indicate that although cytoskeletal systems are not essential for exocyst localization at the PM in the short term, long-term actin disruption leads to changes in exocyst localization and its dynamics at the PM.

Do all exocyst foci harbor secretory vesicles?

The exocyst complex is supposed to function as a vesicle–PM tethering machinery. To address the mechanism of exocyst-complex function, we asked whether the observed exocyst foci also harbor secretory vesicles tethered to the PM. We attempted to visualize secretory vesicles using the secretory marker secGFP (Batoko *et al.*, 2000) but did not observe any vesicle-like events using VAEM (unpublished data). Exocytic vesicles harbor v-SNARE proteins that eventually form SNARE complexes with their PM counterparts. Therefore we tagged VAMP721—a v-SNARE (R-SNARE) expressed in root cells (Uemura *et al.*, 2004; Lipka *et al.*, 2007), which has been used as a marker of exocytosis in plants (Genre *et al.*, 2012)—with GFP and expressed the fusion protein in *Arabidopsis* under the control of its native promoter. Using CLSM, we observed signal in endosomal compartments and a PM signal that was strong at the outer PM of root epidermal cells (Figure 4A). The fusion protein also labeled growing cell plates (Supplemental Figure S1B). The GFP-VAMP721 signal localized to the PM and also to distinct foci, likely vesicles (Allersma *et al.*, 2004), when observed by VAEM. The putative vesicles were moving beneath the PM, and a subpopulation of the foci was tethered at the PM. Dwelling of some foci followed or preceded their movement (Figure 4A). It is possible that

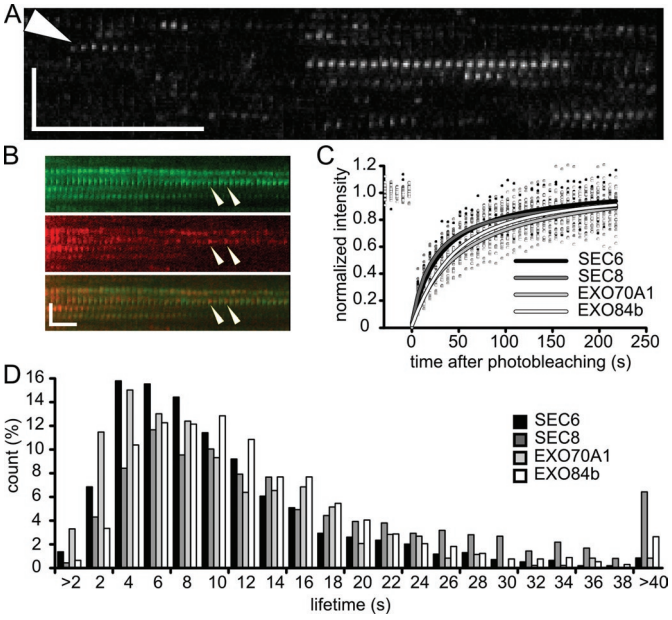

FIGURE 2: Exocyst foci dynamics. (A) A kymographic representation of EXO84b-GFP at the PM of an elongating root epidermal cell. Arrowhead points to lateral movement of EXO84b-GFP in the vertical direction. Horizontal and vertical bars represent 5 s and 3 µm, respectively. (B) A kymographic representation of SEC6-GFP and EXO84b-mRFP colocalization in the exocyst foci. Recruitment of new EXO84b-mRFP molecules is apparent (arrowheads). The horizontal and vertical bars represent 10 s and 2 µm, respectively. (C) FRAP of exocyst subunits at lateral PM of elongating root epidermal cells. Each curve was constructed from ≥10 FRAP experiments; the individual measurements are represented by dots. (D) Histogram showing distribution of exocyst foci lifetimes measured in kymographs; $n \geq 600$ foci for each subunit.

these foci correspond to exocytic and endocytic foci, but we were unable to distinguish between the two types of events.

The pattern of the GFP-VAMP721 foci resembled that of exocyst foci (Figure 4, A and B). We tested the colocalization between GFP-VAMP721 and the exocyst—represented by EXO84b-mRFP, as this construct proved reliable and had stronger signal than SEC6-mRFP. EXO84b-mRFP colocalized with GFP-VAMP721 at the lateral PM but not in the endosome-like compartments when observed by CLSM (Supplemental Figure S1C). When VAEM was used, exocyst foci colocalized with the GFP-VAMP721 putative vesicles tethered at the PM in 21.6% of the foci observed (Figure 4, D and E), whereas the colocalization caused by a random overlap was 10.6%. A portion of the exocyst foci is thus associated with putative secretory vesicles. However, the question remains whether the remaining foci also tether vesicles.

We further attempted to visualize a PM-localized t-SNARE protein. The SYP132 t-SNARE (Qa-SNARE) is expressed ubiquitously during all plant developmental stages, suggesting that it could be involved in constitutive PM trafficking (Uemura *et al.*, 2004; Enami *et al.*, 2009). GFP-tagged SYP132 appeared as a PM signal using CLSM (Figure 4C; Kato *et al.*, 2010). With VAEM, the SYP132-GFP signal localized to motile foci of high density, probably representing SYP132 protein clusters (Figure 4C). Unlike the exocyst subunits, it was difficult to distinguish individual foci and thus impossible to determine their actual density. When we compared the kymographs of exocyst subunits and the SYP132 foci (Figure 4, B and C), it was obvious that SYP132 foci exhibited substantially higher motility, and we did not observe any long-lasting exocyst-like foci in the case of SYP132. Due to the motility and short SYP132 dwelling times, the potential colocalization would not be observable in the time resolution achieved during the sequential imaging of the green and red channels.

If all exocyst foci do tether a membrane-bound vesicle, these would be discernible using electron microscopy. High-pressure freezing, automated freeze-substitution electron microscopy (HPF-AFS) is commonly used to analyze endomembrane processes (Seguí-Simarro *et al.*, 2004), as the sample is fixed within a fraction of a second, thus preserving all endomembrane structures. We fixed the epidermal cells of *Arabidopsis* root tips using HPF-AFS and examined the lateral PM for the presence of tethered vesicles. In total, we analyzed 93.6 µm of the lateral PM of epidermal root cells (Figure 4H). The sections examined were 60 nm thick. The approximate diameter of secretory vesicles in *Arabidopsis* is 50–70 nm (Seguí-Simarro *et al.*, 2004; Ketelaar *et al.*, 2008). Therefore the area of lateral PM examined is roughly 11.2 µm^2 (the length examined multiplied by the sum of the section thickness and the vesicle diameter, as a vesicle cut in half while sectioning will be visible in the micrograph). If all exocyst foci harbored vesicles, we would observe ~18 vesicles (the area examined multiplied by the exocyst foci density, 1.6 µm^{-2}), but instead we observed only 3 vesicles in the vicinity of the lateral PM of epidermal cells (Figure 4, F–I). Recently it was reported (Wang *et al.*, 2010) that the exocyst associates with double-membrane structures that are secreted into the apoplast; however, we observed only structures distantly resembling these compartments—the paramural bodies often found in corners of epidermal cells (Figure 4F).

To test the hypothesis that the exocyst localizes to the PM even without the presence of a vesicle, we used an approach with a higher throughput than transmission electron microscopy imaging and blocked exocytosis using the ARF-GEF inhibitor brefeldin A (BFA), which causes the aggregation of the *trans*-Golgi network and partially inhibits exocytosis (Geldner *et al.*, 2003; Teh and Moore, 2007). After 2-h treatment of 4-d seedlings with 50 µM BFA, the GFP-VAMP721 signal in root epidermal cells aggregated in so-called BFA compartments, and its intensity on the PM decreased, indicating that exocytosis was inhibited (Figure 5). On the contrary, EXO84b, EXO70A1, SEC6, and SEC8 GFP-tagged exocyst subunits did not exhibit such behavior, and their signal persisted completely at the PM (Figure 5). Note that the analysis of VAMP721 VAEM images was very difficult due to the signal of the endomembrane compartments present beneath the plasma membrane. After BFA treatment of VAMP721, the PM signal decreased, whereas the underlying endomembrane particles were still present; therefore we did not analyze the BFA-treated samples using VAEM but used confocal microscopy instead.

In summary, the partial colocalization with the VAMP721 v-SNARE, the lack of tethered vesicles at the lateral PM as examined by HPF-AFS, and the insensitivity of the exocyst to BFA demonstrate that the exocyst foci represent sites of exocyst complex docking at the PM that occur also without the presence of secretory vesicles. Thus the exocyst foci probably form at preexisting sites capable of vesicle tethering.

Exocytosis is decreased in exocyst mutants

The exocyst is an octameric protein complex, and loss-of-function mutations of its subunits result in developmental defects, implying that it needs all of its components for proper functioning. To test whether exocyst foci are altered in cells lacking one of the exocyst components, we expressed the SEC6-GFP subunit in the *exo70A1* exocyst mutant (Synek *et al.*, 2006). We compared

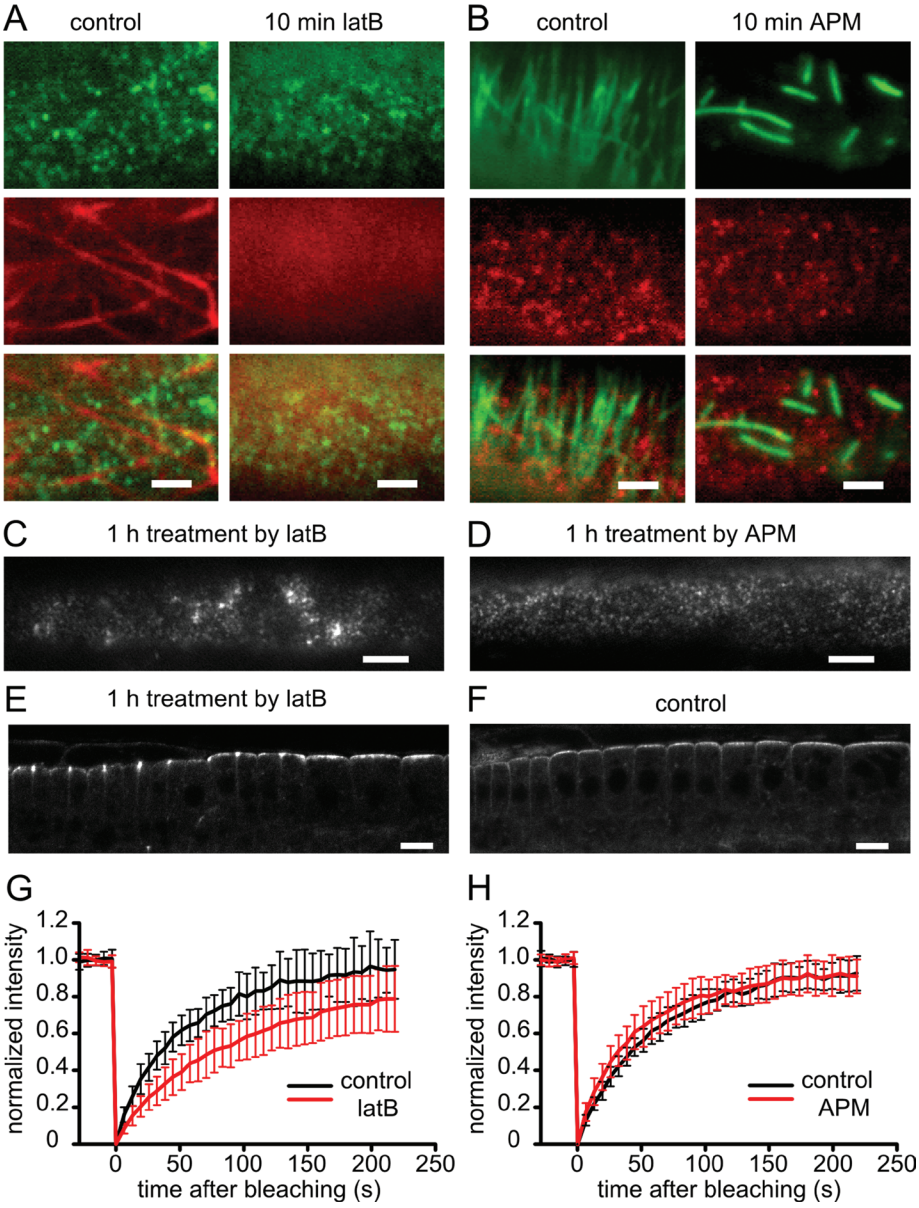

FIGURE 3: EXO84b-GFP and cytoskeleton in root epidermal cells. (A) EXO84B-GFP (green) does not colocalize with actin as visualized by Lifeact-mRFP (red). Short-term actin disruption (10 min, right) does not influence the appearance of exocyst foci. Scale bars, 2 μm. (B) Localization of EXO84b-mRFP (red) and microtubules (green, MAP4-GFP). After 10-min APM treatment, microtubules are disrupted, whereas exocyst foci remain unaffected. Scale bars, 2 μm. (C, D) EXO84b-GFP foci 1 h after disruption of actin (C) and microtubule (D) cytoskeleton. Scale bars, 5 μm. (E, F) EXO84b-GFP in CLSM root sections 1 h after disruption of actin (E) and control (F). Hyperpolarization of the exocyst signal is obvious in E. Scale bars, 10 μm. (G, H) FRAP curves demonstrate retarded recovery of EXO84b-GFP at the PM of the epidermal root cells upon 1-h treatment by latB (G). MT disruption had no effect. Error bars, SDs; $n = 12$ (controls), 20 (latB and APM treatments).

phenotypically wild-type plants (heterozygous and wild type with respect to the *exo70A1* allele) with the mutants. In the latter, the PM incidence of SEC6-GFP foci was decreased, as manifested in a conspicuously decreased density of the foci at the lateral PM of the elongation zone (Figure 6, A and B). The foci sometimes formed clusters at the PM, which were never observed in wild-type controls (Figure 6A).

If the exocyst foci indeed represent PM sites with vesicle-tethering capacity, then the decrease in exocyst foci density should result in decreased exocytosis. In root epidermal cells, GFP-tagged VAMP721 is partitioned between the PM and endomembrane compartments. The strong signal at the lateral PM likely results from intensive exocytosis (Figure 4A). The ratio of the PM and endomembrane signals can then be used as an approximation for ongoing exocytosis. Therefore we examined GFP-VAMP721 in *exo84b* and *exo70A1* exocyst mutants. The *exo84b-1* and *exo84b-2* mutants are dwarf plants with pleiotropic developmental defects (Fendrych *et al.*, 2010). In both lines, the GFP-VAMP721 localization differed dramatically from the wild type: the lateral PM signal was lost, and the protein was present in the cytoplasm and the endomembranes (Figure 6C). We further analyzed the localization of GFP-VAMP721 in the *exo70A1* mutant, which is less severely affected, and its cell types can be directly compared with wild type. In *exo70A1*, lateral PM-domain localization typically decreased and the signal in the endomembrane compartments increased, although some mutant cells resembled wild-type cells. To quantify this observation, we determined the ratio of the lateral PM-domain signal to the entire cytoplasmic signal. This ratio was lower in *exo70A1* mutants than in phenotypically wild-type siblings and wild-type plants (Figure 6D). We were unable to compare the GFP-VAMP721 signal using VAEM microscopy, as the endomembrane compartments accumulated below the PM in the mutant plants hamper such an analysis, similar to the situation in BFA-treated samples (see earlier discussion).

In summary, the absence of the EXO70A1 subunit leads to a decreased recruitment of the SEC6 subunit to the PM. This indicates that the exocyst-docking function was impaired in the *exo70A1*-mutant plants. In turn, exocytosis decreased in these plants, as inferred from the localization of GFP-VAMP721. A plausible explanation of this effect is that the cells face difficulties in exocytosis due to the inability to tether vesicles to the PM. Such inability may well explain morphological and developmental defects of the *exo70A1* mutant.

DISCUSSION

Exocyst localization was described in various model organisms as intense signal in secretory-active PM domains; in *Arabidopsis* roots, the exocyst decorated strongly the outer PM of elongating epidermal cells. The outer epidermal cell domain defines the root–soil interface, and it is a site of active secretion of pectinaceous mucilage (Willats *et al.*, 2001; Langowski *et al.*, 2010). The role of the exocyst in pectinaceous mucilage secretion in the seed coat was described by Kulich *et al.* (2010), and a similar role likely holds in the case of

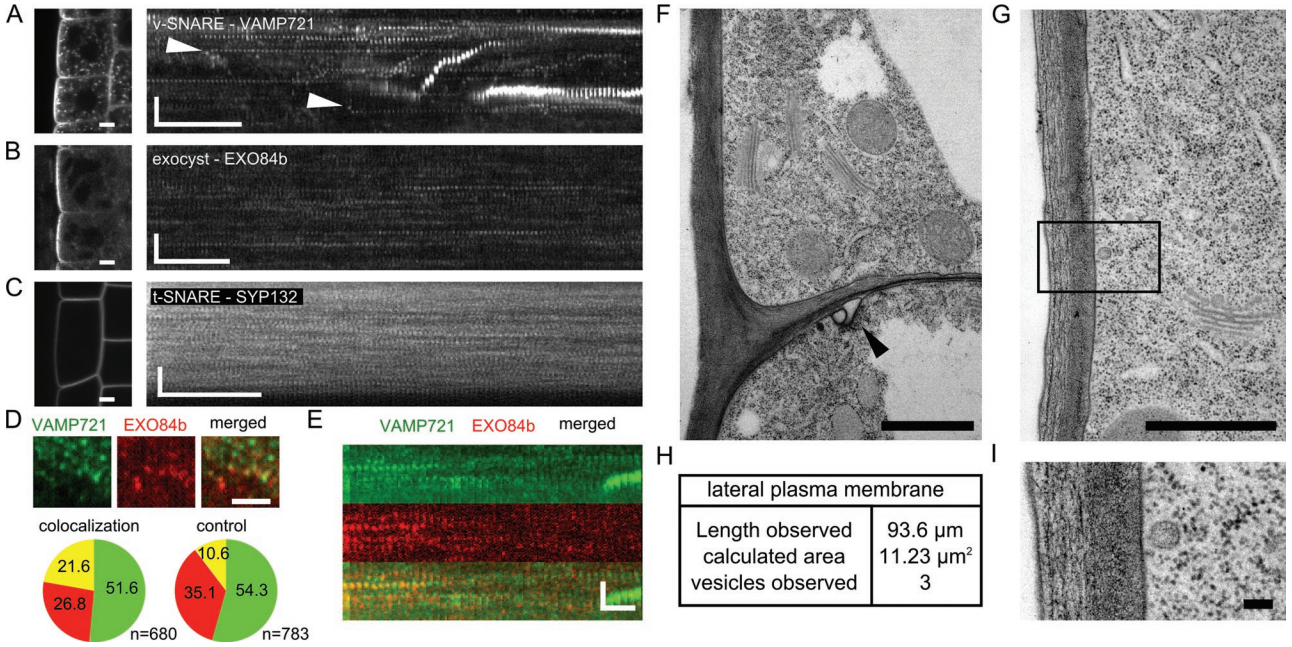

FIGURE 4: Colocalization of exocyst foci with vesicle marker and electron microscopy analysis of the lateral plasma membrane of root epidermal cells. (A–C) Comparison of VAMP721 (A), exocyst foci (B), and SYP132-GFP (C) CLSM localization (left) and dynamics visualized by VAEM (right). GFP-VAMP721 localizes to epidermal PM and endosomes and EXO84b-GFP signal is prominent at the outer epidermal PM, whereas SYP132-GFP is evenly distributed along the entire PM; the seemingly stronger signal of the intercellular membranes results from summing of the adjacent PM signal. Kymographs demonstrate that VAMP721 and exocyst label PM-localized foci with similar appearance (A, B). VAMP721 foci dwelling at the PM are preceded by movement of the foci (arrowheads). Motile foci and endosomes are visible in the kymograph (B). SYP132-GFP (C) is highly dynamic compared with EXO84b-labeled foci. Scale bars, 5 µm (left); horizontal and vertical bars (right) represent 5 s and 3 µm, respectively. (D) Colocalization of GFP-VAMP721 and EXO84b-mRFP foci (scale bar, 2 µm), and quantification (%) of the colocalization (left). The random overlap quantification is shown on the right. Note the weak PM signal of GFP-VAMP721 apart from the larger foci. (E) Kymographic representation of the colocalization between GFP-VAMP721 and EXO84b-mRFP; horizontal and vertical bars represent 10 s and 2 µm, respectively. (F, G) HPF-AFS electron microscopy analysis of the lateral PM of *Arabidopsis* root epidermal cells. (H) Table summarizing the length and area of lateral PM analyzed and number of visible vesicles. From the actual vesicle number observed it is clear that only a subset of exocyst foci are tethering a vesicle. Numerous Golgi and endomembranes are apparent in F, but no vesicles are tethered below the lateral PM. In the lower cell, paramural bodies are present (arrowhead). An example of vesicle tethered at the PM is shown in G; note also the presence of numerous vesicles in the cytoplasm close to the Golgi. (I) Magnified inset from (G); the distance of the vesicle from the PM is 23 nm. Scale bars, 1 µm in F and G and 100 nm in I.

the root epidermis. In postmitotic cells, the exocyst refocuses to the maturing cell wall, another domain with high secretion demands (Fendrych *et al.*, 2010). Here, using VAEM, we achieved a new level of spatiotemporal resolution and characterized the exocyst dynamics in PM-localized foci.

We showed that SEC6-, SEC8-, and EXO84b-positive foci colocalize. There was, however, also a significant proportion of GFP-only labeled foci. For technical reasons, GFP and mRFP channels were imaged sequentially, resulting in an approximately 1-s delay between imaging of the two channels, explaining part of the noncolocalizing foci. Although the mRFP-tagged protein expression was driven by the 35S constitutive promoter, the expression levels were low, and the localization pattern was very similar when compared the 35S promoter with the native-promoter–driven constructs (EXO84b-RFP, SEC6-RFP). In fact, the mRFP signal hit the detection limit of the microscope setup. The mRFP protein has a lower quantum yield and bleaches faster than GFP (Dixit *et al.*, 2006), and in our microscope setup, the mRFP signal was photobleached rapidly, explaining another part of the GFP-only–labeled foci. It is also possible that GFP-tagged subunits are incorporated into exocyst complexes more easily than the mRFP-tagged ones, perhaps due to the weak ability of the GFP to dimerize (Zacharias *et al.*, 2002). The exocyst foci (represented by SEC8) differed from the endocytic sites marked by dynamin-related protein 1C (Konopka and Bednarek, 2008a; Konopka *et al.*, 2008). The density of the foci was similar for all exocyst subunits tested, and it decreased with the distance from the root apical meristem.

We further tested the dependence of exocyst localization and dynamics on actin and MT cytoskeletons. Although the exocyst was shown to localize to MT in opisthokont cells (Vega and Hsu, 2001; Wang *et al.*, 2004), we observed neither significant colocalization nor an effect of MT disruption on exocyst foci appearance. The immediate exocyst localization was actin independent, but long-term actin disruption led to changes in exocyst foci appearance and dynamics. This was probably due to unequal distribution of the foci and compartments that are sources of exocytic vesicles. The delivery of cellulose–synthase complexes to the PM was not microtubule dependent (Gutierrez *et al.*, 2009), and similar to our results, upon actin disruption, the pattern of distribution of the complexes at the PM was disrupted, likely reflecting the irregular distribution of

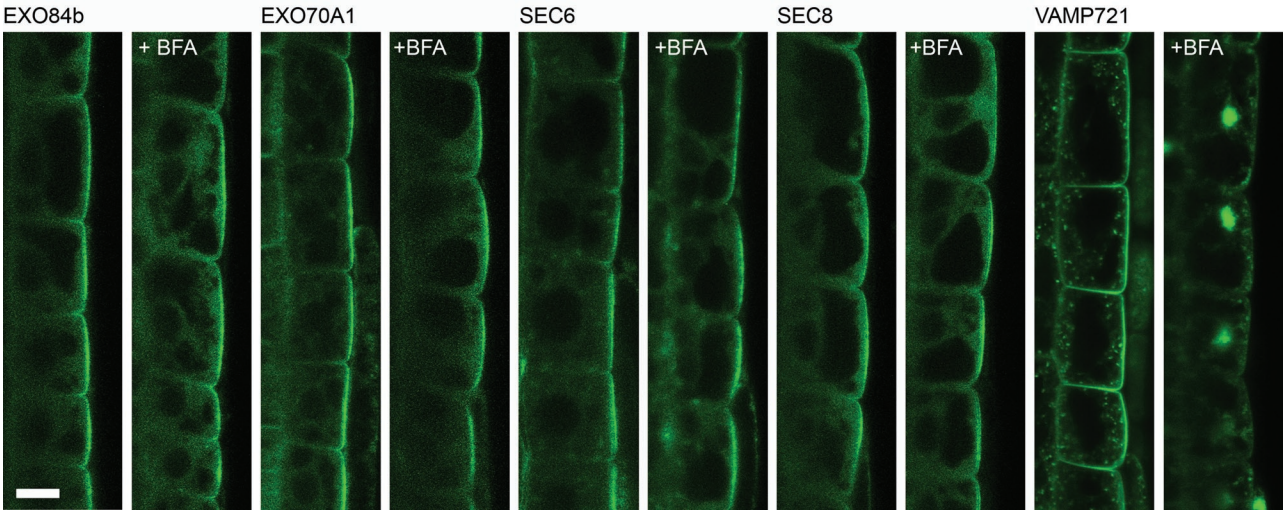

FIGURE 5: The exocyst is insensitive to brefeldin A treatment. Plants expressing exocyst subunits and VAMP721 GFP fusions were treated with BFA for 2 h as indicated. The exocyst subunits remained localized on the lateral PM in the root epidermal cells, whereas the VAMP721 aggregated in BFA compartments. Scale bars, 10 µm.

vesicle-producing compartments (Crowell *et al.*, 2009; Gutierrez *et al.*, 2009). These results agree with the notion that fission yeast polarity and morphogenesis are cooperatively guided by actin and the exocyst, albeit in a redundant manner (Bendezú and Martin, 2010). In addition, it seems that the fission yeast exocyst holocomplex is delivered to the growing ends of cells by the F-actin network (Bendezú *et al.*, 2012).

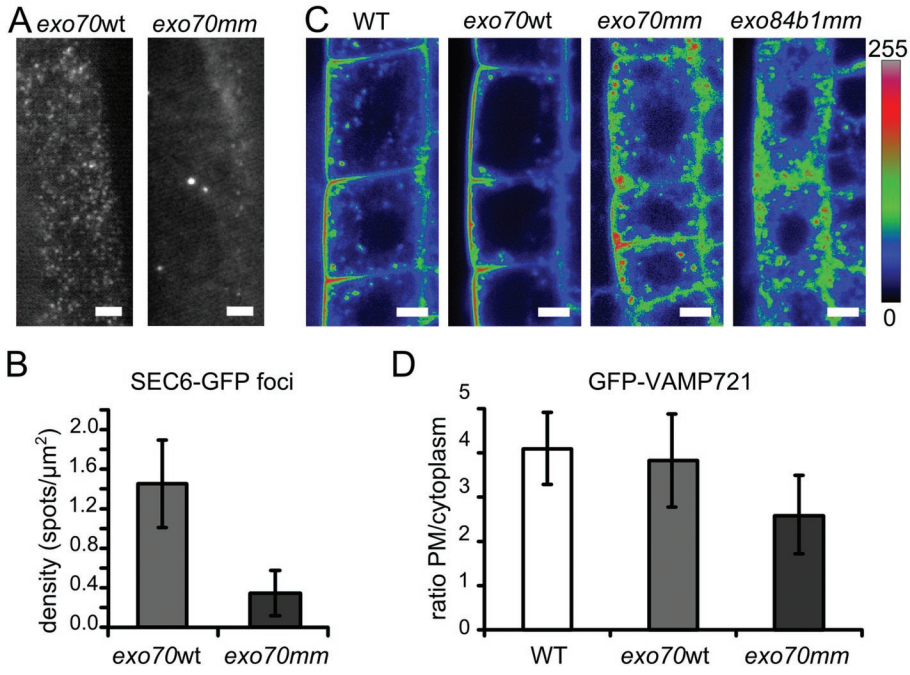

FIGURE 6: Mutations in exocyst subunits decrease the incidence of exocyst foci at the PM and lead to a decrease in exocytosis. (A) SEC6-GFP exocyst foci in wild-type and *exo70A1*-mutant root epidermal cells; scale bars, 2 µm. (B) quantification of SEC6-GFP foci density in *exo70A1* wild-type and mutant cells; error bars, SDs; $n = 23$ and 12 cells for *exo70A1mm* and exo70A1 wild type, respectively. (C) GFP-VAMP721 localizes to the lateral PM and endomembranes in the wild type and *exo70A1* phenotypic wild-type cells. In *exo70A1* and *exo84b1* exocyst mutants, GFP-VAMP721 localization to the lateral PM decreases, and, in turn, the signal of endomembrane compartment increases. Calibration bar of the color coding is shown on the right; scale bars, 5 µm. (D) Quantification of the lateral PM domain/cytoplasmic signal intensity ratio in wild-type, *exo70A1* wild-type, and *exo70A1* mutants. The *exo84b* mutants were not quantified due to the lack of signal at the PM. $n = 48$ cells in 18 seedlings (wild type), $n = 54$ cells in 18 seedlings (*exo70A1* wild type), and $n = 45$ cells in 16 seedlings (*exo70A1* mutants); error bars, SDs.

The assembly and dynamics of exocyst subunits has been a matter of a debate. The seminal model of Peter Novick, based on yeast data, proposes consecutive assembly of exocyst subcomplexes on the vesicle (mediated by Sec15–Sec4 interaction) and on the target PM domain (Sec3 and Exo70). Full complex assembly then results in vesicle tethering (Bröcker *et al.*, 2010). Alternatively, the exocyst might function as a particle preassembled at the plasma membrane that is activated by Rho GTPases to trigger tethering (Wu *et al.*, 2008). The latter model is also supported by the finding that after specific mutations of the yeast Sec6 subunit, the exocyst is released from PM as a complete particle (Songer and Munson, 2009). Theoretically, the exocyst assembly could be observed by colocalization of differentially labeled subunits in the PM foci. Nevertheless, this was impossible using our microscope setup due to the low time resolution caused by sequential imaging. However, the fact that dynamics and density at the PM were similar for all subunits tested, including EXO70A1—which would be expected to "wait" as a landmark at the PM based on the consecutive assembly model—supports the hypothesis of the exocyst function as a preassembled particle. This inference is strengthened by the fact that the exocyst subunits were present at the PM even without the tethered vesicle (also upon addition of BFA). A recent report on the preassembled exocyst holocomplex (including the

Sec3 subunit) delivered to the PM by F-actin in fission yeast strongly supports the possibility of the exocyst holocomplex functioning as a particle in vesicle tethering (Bendezú *et al.*, 2012).

Our study in plants presents data showing that the exocyst localized in distinct foci. The intriguing question is whether exocyst foci correspond to secretory vesicles tethered to the PM in *Arabidopsis* cells. We found only partial colocalization with the secretory vesicle marker VAMP721 v-SNARE. Capturing of exocytosis events by electron microscopy is very rare. In plants, vesicle tethering has not been addressed in detail, but there are reports showing vesicles or vesicle clusters associated with the PM (Toyooka *et al.*, 2009). As a complementary approach to fluorescence microscopy, we used electron microscopy to analyze the number of vesicles actually tethered at the PM. Tethering might occur at distance greater than half of the vesicle size, but the presumed exocyst dimensions are ~13 × 30 nm (Hsu *et al.*, 1998); therefore the tethered vesicle should be visible in the proximity of PM connected to the exocyst foci. Our electron microscopy results demonstrated that there are fewer vesicles tethered at the PM than there are exocyst foci. Therefore we conclude that either vesicles are bound to the exocyst foci for a very short time or only a subset of exocyst foci actually tether a vesicle during its existence. We are not able to distinguish between these two possibilities; in both scenarios, the exocyst is present at the PM even without the actual presence of a secretory vesicle. This conclusion is further supported by the insensitivity of exocyst-subunit PM localization to BFA treatment. This indicates that although exocytosis decreased, exocyst subunits were still able to dock at the PM.

We further compared the localization of the PM-localized SYP132 t-SNARE with the exocyst (Uemura *et al.*, 2004; Enami *et al.*, 2009). In animal cells, syntaxins assemble into clusters at sites of secretory granules (Barg *et al.*, 2010). We hoped to elucidate the time at which t-SNAREs associate with the fusion site and the portion of the putative exocytic foci that actually end up in a successful vesicle fusion. Comparison of SYP132 and exocyst foci localization showed that the t-SNARE is ubiquitously present throughout the entire PM, whereas the exocytic sites are selected by the exocyst complex located at secretory-active domains (Žárský *et al.*, 2009).

Finally, we analyzed exocyst localization in a mutant of the EXO70A1 exocyst subunit, a highly expressed member of the *Arabidopsis* EXO70 family (Synek *et al.*, 2006). In this mutant, density of exocyst foci at the PM decreased substantially, indicating that exocyst function is likely reduced in mutant cells. The hypothesis that the marked decrease of exocyst foci resulted in decreased exocytosis was supported by a decrease of a secretory vesicle marker (VAMP721-GFP) at the PM of the *exo*70A1 and *exo*84b mutants, suggesting impaired exocytosis in these cells. This result agrees with the work of Tsuboi *et al.* (2005), who showed decreased vesicle docking in exocyst-mutant cells.

In summary, we provided insights into the dynamics of exocyst-complex subunits docking at the plant plasma membrane. We propose that the exocyst serves to increase vesicle-tethering probability at PM domains and is able to localize—most probably as a particle—to the PM without the associated vesicle.

MATERIALS AND METHODS

Optical microscopy

We used a Leica DMI6000 microscope (Leica Microsystems, Vienna, Austria) with total internal reflection fluorescence illumination and an HCX PL APO 100.0×/1.46 oil objective. The penetration depth was set to 90–250 nm, roughly corresponding to angles of 64–61°, and the exposure time to ~80–200 ms (300 ms for mRFP and mOrange). Note that the set penetration depths do not necessarily reflect the actual physical penetration depths, due to the intricate optical system of interfaces with various refractive indexes: the glass–medium, medium–cell wall, and cell wall–cytoplasm interfaces. Excitation at 488 nm and the GFP filter were used for imaging of GFP. Excitation at 488 and 560 nm, the QuadP-T cube, and 525/36 and 600/32 filters were used for GFP/mRFP and GFP/mOrange sequential imaging. Relative focus correction was used for colocalization imaging to compensate for the fact that different wavelengths appear at different focal depths. The system, equipped with a DFC350FXR2 camera, was controlled by LAS AF software (Leica).

FRAP experiments were performed using the Zeiss LSM 5 DUO CLSM (Zeiss, Jena, Germany) with the Zeiss C-Apochromat 40×/1.2 water-corrected objective. All images were acquired using identical settings: image size was 500 × 200 pixels; the region of interest (70 × 20 pixels) was bleached using 10 iterations of a 489-nm laser at 100% laser power; and 5 and 35 frames by 6.5-s steps were acquired before and after bleaching, respectively.

HPF-AFS and electron microscopy

Root tips of 5-d-old seedlings of *A. thaliana* were excised, immersed in 20% (wt/vol) bovine serum albumin, and frozen immediately in a high-pressure freezer (EM PACT; Leica Microsystems). Freeze substitution was carried out using a Leica EM AFS (Leica Microsystems) in dry acetone containing 0.1% uranyl acetate, 1% (wt/vol) OsO_4, and 0.2% glutaraldehyde over a 4-d period as follows: –90°C for 54 h, 2°C/h increase for 15 h, –60°C for 8 h, 2°C/h increase for 15 h, and –30°C for 8 h. Samples were then slowly warmed to 4°C, infiltrated stepwise over 3 d at 4°C in Spurr's resin, and embedded in capsules. The polymerization was performed at 70°C for 16 h. Ultrathin sections were made using an ultramicrotome (Leica EM UC6) and poststained in a Leica EM AC20 for 40 min in uranyl acetate at 20°C and for 10 min in lead stain at 20°C. Grids were viewed with a JEM 1010 transmission electron microscope (JEOL, Tokyo, Japan) operating at 80 kV.

Molecular cloning

SEC6 and EXO84b were transferred into pK7RWG2 (Karimi *et al.*, 2002) binary vector by the LR Clonase II enzyme mix (Invitrogen, Carlsbad, CA).

Lifeact marker (Riedl *et al.*, 2008) was amplified using Lifeact5 and Lifeact3 primers in a reaction without a template DNA. The product was further reamplified using attB1 and attB2 primers to flank it with the attB sites. Resulting product was transferred into the pDONR207 vector (Invitrogen) using the BP Clonase II (Invitrogen) and further to the pK7RWG2 vector by the LR Clonase II (Invitrogen).

VAMP721 (AT1G04750) was cloned by the three-template PCR method (Tian *et al.*, 2004). The VAMP721 promoter region and VAMP721 gene were amplified from *A. thaliana* genomic DNA by using P1 and P2, and P5 and P6 primers, respectively; the GFP gene was amplified from the pGWB6 vector (Nakagawa *et al.*, 2007) by using P3 and P4 primers. In a subsequent PCR, resulting products were mixed and amplified using attB1 and attB2 primers. Product of this three-template reaction was transferred into pDONR207 and further to the pGWB1 binary vector (Nakagawa *et al.*, 2007) by BP Clonase II and LR Clonase II enzyme mix, respectively. The construct was verified by sequencing; the promoter region lacked the initial 400 base pairs, resulting in ~800–base pair promoter region. GFP-VAMP721 was transformed into *A. thaliana* expressing EXO84b-mRFP using the floral dip method.

Lifeact5	AAAAAAGCAGGCTCCACCATGGGTGTCGCA-GATTTGATCAAGAAATTC
Lifeact3	AGAAAGCTGGGTCTTCTTCCTTTGAGATGCTTTC-GAATTTCTTGATCA
attB1	GGGGACAAGTTTGTACAAAAAAGCAGGCT
attB2	GGGGACCACTTTGTACAAGAAAGCTGGGT
P1	AAAAAGCAGGCTAACGAAACCTAAGAACACCAC
P2	GCCCTTGCTCACCATTTTTTCTTTACCT-TAAATCTCC
P3	TAAGGTAAAGAAAAAATGGTGAGCAAGGGCGAG
P4	GGCCCCAGCGGCCGCAGCAGCACCAGCGTA-CAGCTCGTCCATGCC
P5	CTGCTGCGGCCGCTGGGGCCATGGCGCAA-CAATCGTTGATC
P6	AGAAAGCTGGGTCTTAACACTTAAACCCATG-GCAAAC

TABLE 1: Primers used.

All PCRs were performed using the Phusion polymerase (Finnzymes, Thermo Scientific, Vantaa, Finland). Primers used are listed in Table 1.

Plant material

The Columbia-0 ecotype of *A. thaliana* was transformed using the floral dip method (Clough and Bent, 1998).

Seeds of *A. thaliana* expressing SYP132 were kindly provided by M. H. Sato (Graduate School of Life and Environmental Sciences, Kyoto Prefectural University, Japan) and DRP1C-mOrange by S. Bednarek (Department of Biochemistry, University of Wisconsin–Madison).

F1 generation of crosses between plants expressing GFP- and mRFP- or GFP- and mOrange-tagged proteins was used for evaluation of possible colocalization; in the case of VAMP721–EXO84b colocalization, T2-generation seedlings were used. To observe SEC6-GFP foci in the *exo70A1* mutant, we transformed the *exo70A1-1* line with the SEC6-GFP construct using the floral dip method. In the T2 generation, phenotypically homozygous plants were selected and compared with phenotypically wild-type siblings.

Four-day-old *Arabidopsis* plantlets grown on vertical agar plates were transferred with a block of agar beneath into a minute droplet of half-strength Murashige and Skoog medium (½ MS) supplemented with 1% (wt/vol) sucrose in a LabTekII chambered coverglass and observed. Five-day-old seedlings were used for FRAP experiments.

For cytoskeleton treatment, 10 mM latrunculin B (Molecular Probes, Eugene, OR) in dimethyl sulfoxide and 100 mM amiprophos methyl (APM; Sigma-Aldrich, St. Louis, MO) in ethanol were used. Seedlings were transferred into ½ MS containing a 1:1000 dilution of the appropriate drug or equivalent volume of the solvent in controls, incubated for 10 min or 1 h, respectively, and observed.

The BFA experiment was conducted as follows: 4-d-old seedlings expressing GFP-tagged exocyst subunits or VAMP721, respectively, were treated with 50 mM brefeldin A diluted 1:1000 in ½ MS liquid medium. Images of epidermal cells at root transition zone were taken after 2-h treatment.

Image analysis

All images were analyzed using ImageJ software (National Institutes of Health, Bethesda, MD). Root growth was compensated using the CorrectStackDrift.txt macro (http://rsbweb.nih.gov/ij/macros/examples/). Density of foci was determined in a rectangle of ~50 μm^2 using the Cell Counter ImageJ plug-in. GFP/mRFP and GFP/mOrange colocalization was analyzed as follows: the first three images in a time series were averaged to enhance the signal of the stable foci. Only cell areas where both channels were focused properly were used for evaluation. Random overlap was determined in images where one of the channels was shifted by 30 pixels. Colocalization was determined by evaluating each labeled spot by eye in the assayed area and counted using the Cell Counter ImageJ plug-in.

Kymographs were constructed from five-pixel-wide rectangles from each time point concatenated consecutively. To determine exocyst dynamics, series obtained in 0.5-s intervals were used to ensure proper coverage of both the short-time and the long-lasting events; lengths of exocytic events were measured manually in kymographs.

FRAP images were corrected for root growth, and intensities were normalized as follows:

$$I_t = \left[(A_t/C_t) - (A_b/C_b)\right] / \left[\mathrm{Av} - (A_b/C_b)\right]$$

where A_t is the intensity in the bleached area at time t; C_t is the intensity in the control, nonbleached area; A_b and C_b are the intensities in the bleached and unbleached areas, respectively, immediately after the bleaching; and Av is the average A_t/C_t intensity ratio in the five frames before bleaching.

Electron micrographs of epidermal root cells were checked for the presence of vesicles in the PM vicinity, and the outer PM length was measured.

Evaluation of GFP-VAMP721 intensities at the PM and cytoplasm was achieved by creating a region of interest encompassing the entire cytoplasm and lateral PM domain, respectively; mean intensity was recorded, and the ratio was calculated.

All data were processed using the Gnumeric spreadsheet (http://projects.gnome.org/gnumeric/), and FRAP curves were fitted using Gnuplot (www.gnuplot.info/) with the equation

$$f(x) = a + b^{*}\arctan[c(x - d)]$$

Figures were assembled in ImageJ, GIMP (www.gimp.org/), and Inkscape (www.inkscape.org) software, and histograms were adjusted to obtain the best signal-to-noise ratio.

ACKNOWLEDGMENTS

This work was supported by Grant Agency of the Czech Republic/Czech Science Foundation Projects P305/11/1629. We thank Martin Potocký and Jan Petrášek for helpful discussions, Pavel Hejbal for help with Gnuplot, and S. Bednarek for kindly providing experimental material. M.F. thanks the developers of Ubuntu Linux, Gnome, GIMP, and Inkscape.

REFERENCES

Allersma MW, Wang L, Axelrod D, Holz RW (2004). Visualization of regulated exocytosis with a granule-membrane probe using total internal reflection microscopy. Mol Biol Cell 15, 4658–4668.

Barg S, Knowles M, Chen X, Midorikawa M, Almers W (2010). Syntaxin clusters assemble reversibly at sites of secretory granules in live cells. Proc Natl Acad Sci USA 107, 20804–20809.

Batoko H, Zheng HQ, Hawes C, Moore I (2000). A rab1 GTPase is required for transport between the endoplasmic reticulum and Golgi apparatus and for normal Golgi movement in plants. Plant Cell 12, 2201–2218.

Battey N, James N, Greenland A, Brownlee C (1999). Exocytosis and endocytosis. Plant Cell 11, 643–660.

Bendezú FO, Martin SG (2010). Actin cables and the exocyst form two independent morphogenesis pathways in the fission yeast. Mol Biol Cell 22, 44–53.
Bendezú FO, Vincenzetti V, Martin SG (2012). Fission yeast Sec3 and Exo70 are transported on actin cables and localize the exocyst complex to cell poles. PLoS One 7, e40248.
Boyd C, Hughes T, Pypaert M, Novick P (2004). Vesicles carry most exocyst subunits to exocytic sites marked by the remaining two subunits, Sec3p and Exo70p. J Cell Biol 167, 889–901.
Bröcker C, Engelbrecht-Vandré S, Ungermann C (2010). Multisubunit tethering complexes and their role in membrane fusion. Curr Biol 20, R943–R952.
Cai H, Reinisch K, Ferro-Novick S (2007). Coats, tethers, Rabs, and SNAREs work together to mediate the intracellular destination of a transport vesicle. Dev Cell 12, 671–682.
Clough SJ, Bent AF (1998). Floral dip: a simplified method for *Agrobacterium*-mediated transformation of *Arabidopsis thaliana*. Plant J 16, 735–743.
Cole RA, Synek L, Žárský V, Fowler JE (2005). SEC8, a subunit of the putative *Arabidopsis* exocyst complex, facilitates pollen germination and competitive pollen tube growth. Plant Physiol 138, 2005–2018.
Crowell EF, Bischoff V, Desprez T, Rolland A, Stierhof Y-D, Schumacher K, Gonneau M, Höfte H, Vernhettes S (2009). Pausing of Golgi bodies on microtubules regulates secretion of cellulose synthase complexes in *Arabidopsis*. Plant Cell 21, 1141–1154.
Dixit R, Cyr R, Gilroy S (2006). Using intrinsically fluorescent proteins for plant cell imaging. Plant J 45, 599–615.
Enami K, Ichikawa M, Uemura T, Kutsuna N, Hasezawa S, Nakagawa T, Nakano A, Sato MH (2009). Differential expression control and polarized distribution of plasma membrane-resident SYP1 SNAREs in *Arabidopsis thaliana*. Plant Cell Physiol 50, 280–289.
Fendrych M *et al.* (2010). The *Arabidopsis* exocyst complex is involved in cytokinesis and cell plate maturation. Plant Cell 22, 3053–3065.
Finger FP, Hughes TE, Novick P (1998). Sec3p is a spatial landmark for polarized secretion in budding yeast. Cell 92, 559–571.
Fujimoto M, Arimura S, Ueda T, Takanashi H, Hayashi Y, Nakano A, Tsutsumi N (2010). *Arabidopsis* dynamin-related proteins DRP2B and DRP1A participate together in clathrin-coated vesicle formation during endocytosis. Proc Natl Acad Sci USA 107, 6094–6099.
Geldner N, Anders N, Wolters H, Keicher J, Kornberger W, Muller P, Delbarre A, Ueda T, Nakano A, Jürgens G (2003). The *Arabidopsis* GNOM ARF-GEF mediates endosomal recycling, auxin transport, and auxin-dependent plant growth. Cell 112, 219–230.
Genre A, Ivanov S, Fendrych M, Faccio A, Žárský V, Bisseling T, Bonfante P (2012). Multiple exocytotic markers accumulate at the sites of perifungal membrane biogenesis in *Arbuscular mycorrhizas*. Plant Cell Physiol 53, 244–255.
Gromley A, Yeaman C, Rosa J, Redick S, Chen C-T, Mirabelle S, Guha M, Sillibourne J, Doxsey SJ (2005). Centriolin anchoring of exocyst and SNARE complexes at the midbody is required for secretory-vesicle-mediated abscission. Cell 123, 75–87.
Guo W, Grant A, Novick P (1999a). Exo84p is an exocyst protein essential for secretion. J Biol Chem 274, 23558–23564.
Guo W, Roth D, Walch-Solimena C, Novick P (1999b). The exocyst is an effector for Sec4p, targeting secretory vesicles to sites of exocytosis. EMBO J 18, 1071–1080.
Guo W, Tamanoi F, Novick P (2001). Spatial regulation of the exocyst complex by Rho1 GTPase. Nat Cell Biol 3, 353–360.
Gutierrez R, Lindeboom JJ, Paredez AR, Emons AMC, Ehrhardt DW (2009). *Arabidopsis* cortical microtubules position cellulose synthase delivery to the plasma membrane and interact with cellulose synthase trafficking compartments. Nat Cell Biol 11, 797–806.
Hála M *et al.* (2008). An exocyst complex functions in plant cell growth in *Arabidopsis* and tobacco. Plant Cell 20, 1330–1345.
He B, Xi F, Zhang X, Zhang J, Guo W (2007). Exo70 interacts with phospholipids and mediates the targeting of the exocyst to the plasma membrane. EMBO J 26, 4053–4065.
Heider M, Munson M (2012). Exorcising the exocyst complex. Traffic 13, 898–907.
Hsu SC, Hazuka CD, Roth R, Foletti DL, Heuser J, Scheller RH (1998). Subunit composition, protein interactions, and structures of the mammalian brain sec6/8 complex and septin filaments. Neuron 20, 1111–1122.
Karimi M, Inzé D, Depicker A (2002). GATEWAY vectors for *Agrobacterium*-mediated plant transformation. Trends Plant Sci 7, 193–195.
Kato N, Fujikawa Y, Fuselier T, Adamou-Dodo R, Nishitani A, Sato MH (2010). Luminescence detection of SNARE–SNARE interaction in *Arabidopsis* protoplasts. Plant Mol Biol 72, 433–444.
Ketelaar T, Galway ME, Mulder BM, Emons AMC (2008). Rates of exocytosis and endocytosis in *Arabidopsis* root hairs and pollen tubes. J Microsc 231, 265–273.
Konopka CA, Backues SK, Bednarek SY (2008). Dynamics of *Arabidopsis* dynamin-related protein 1C and a clathrin light chain at the plasma membrane. Plant Cell 20, 1363–1380.
Konopka CA, Bednarek SY (2008a). Comparison of the dynamics and functional redundancy of the Arabidopsis dynamin-related isoforms DRP1A and DRP1C during plant development. Plant Physiol 147, 1590–1602.
Konopka Ca, Bednarek SY (2008b). Variable-angle epifluorescence microscopy: a new way to look at protein dynamics in the plant cell cortex. Plant J 53, 186–196.
Kulich I, Cole R, Drdová E, Cvrčková F, Soukup A, Fowler J, Žárský V (2010). *Arabidopsis* exocyst subunits SEC8 and EXO70A1 and exocyst interactor ROH1 are involved in the localized deposition of seed coat pectin. New Phytol 188, 615–625.
Langowski L, Rčžička K, Naramoto S, Kleine-Vehn J, Friml J (2010). Trafficking to the outer polar domain defines the root-soil interface. Curr Biol 20, 904–908.
Lavy M, Bloch D, Hazak O, Gutman I, Poraty L, Sorek N, Sternberg H, Yalovsky S (2007). A novel ROP/RAC effector links cell polarity, root-meristem maintenance, and vesicle trafficking. Curr Biol 17, 947–952.
Lipka V, Kwon C, Panstruga R (2007). SNARE-ware: the role of SNARE-domain proteins in plant biology. Annu Rev Cell Dev Biol 23, 147–174.
Lipschutz JH, Guo W, O'Brien LE, Nguyen YH, Novick P, Mostov KE (2000). Exocyst is involved in cystogenesis and tubulogenesis and acts by modulating synthesis and delivery of basolateral plasma membrane and secretory proteins. Mol Biol Cell 11, 4259–4275.
Marc J, Granger C, Brincat J, Fisher D, Kao T, McCubbin A, Cyr R (1998). A GFP-MAP4 reporter gene for visualizing cortical microtubule rearrangements in living epidermal cells. Plant Cell 10, 1927–1940.
Nakagawa T, Kurose T, Hino T, Tanaka K, Kawamukai M, Niwa Y, Toyooka K, Matsuoka K, Jinbo T, Kimura T (2007). Development of series of gateway binary vectors, pGWBs, for realizing efficient construction of fusion genes for plant transformation. J Biosci Bioeng 104, 34–41.
Novick P, Field C, Schekman R (1980). Identification of 23 complementation groups required for post-translational events in the yeast secretory pathway. Cell 21, 205–215.
Pečenková T, Hála M, Kulich I, Kocourková D, Drdová E, Fendrych M, Toupalová H, Žárský V (2011). The role for the exocyst complex subunits Exo70B2 and Exo70H1 in the plant–pathogen interaction. J Exp Bot 62, 2107–2116.
Riedl J *et al.* (2008). Lifeact: a versatile marker to visualize F-actin. Nat Methods 5, 605–607.
Robinson NGG, Guo L, Imai J, Toh-e A, Matsui Y, Tamanoi F (1999). Rho3 *of Saccharomyces cerevisiae*, which regulates the actin cytoskeleton and exocytosis, is a GTPase which interacts with Myo2 and Exo70. Mol Cell Biol 19, 3580–3587.
Seguí-Simarro JM, Austin JR 2nd, White EA, Staehelin LA (2004). Electron tomographic analysis of somatic cell plate formation in meristematic cells of *Arabidopsis* preserved by high-pressure freezing. Plant Cell 16, 836–856.
Sivaram MVS, Saporita JA, Furgason MLM, Boettcher AJ, Munson M (2005). Dimerization of the exocyst protein Sec6p and its interaction with the t-SNARE Sec9p. Biochemistry 44, 6302–6311.
Söllner T, Whiteheart SW, Brunner M, Erdjument-Bromage H, Geromanos S, Tempst P, Rothman JE (1993). SNAP receptors implicated in vesicle targeting and fusion. Nature 362, 318–324.
Songer JA, Munson M (2009). Sec6p anchors the assembled exocyst complex at sites of secretion. Mol Biol Cell 20, 973–982.
Synek L, Schlager N, Eliáš M, Quentin M, Hauser MT, Žárský V (2006). AtEXO70A1, a member of a family of putative exocyst subunits specifically expanded in land plants, is important for polar growth and plant development. Plant J 48, 54–72.
Teh O-K, Moore I (2007). An ARF-GEF acting at the Golgi and in selective endocytosis in polarized plant cells. Nature 448, 493–496.
Tian GW *et al.* (2004). High-throughput fluorescent tagging of full-length *Arabidopsis* gene products in planta. Plant Physiol 135, 25–38.
Toyooka K, Goto Y, Asatsuma S, Koizumi M, Mitsui T, Matsuoka K (2009). A mobile secretory vesicle cluster involved in mass transport from the Golgi to the plant cell exterior. Plant Cell 21, 1212–1229.

Tsuboi T, Ravier Ma, Xie H, Ewart M-A, Gould GW, Baldwin Sa, Rutter GA (2005). Mammalian exocyst complex is required for the docking step of insulin vesicle exocytosis. J Biol Chem 280, 25565–25570.

Uemura T, Ueda T, Ohniwa RL, Nakano A, Takeyasu K, Sato MH (2004). Systematic analysis of SNARE molecules in *Arabidopsis*: dissection of the post-Golgi network in plant cells. Cell Struct Funct 29, 49–65.

Vega IE, Hsu SC (2001). The exocyst complex associates with microtubules to mediate vesicle targeting and neurite outgrowth. J Neurosci 21, 3839–3848.

Wang J, Ding Y, Hillmer S, Miao Y, Lo SW, Wang X, Robinson DG, Jiang L (2010). EXPO, an exocyst-positive organelle distinct from multivesicular endosomes and autophagosomes, mediates cytosol to cell wall exocytosis in *Arabidopsis* and tobacco cells. Plant Cell 22, 4009–4030.

Wang S, Liu Y, Adamson CL, Valdez G, Guo W, Hsu SC (2004). The mammalian exocyst, a complex required for exocytosis, inhibits tubulin polymerization. J Biol Chem 279, 35958–35966.

Willats WG, McCartney L, Knox JP (2001). In-situ analysis of pectic polysaccharides in seed mucilage and at the root surface of *Arabidopsis thaliana*. Planta 213, 37–44.

Wu H, Rossi G, Brennwald P (2008). The ghost in the machine: small GTPases as spatial regulators of exocytosis. Trends Cell Biol 18, 397–404.

Zacharias DA, Violin JD, Newton AC, Tsien RY (2002). Partitioning of lipid-modified monomeric GFPs into membrane microdomains of live cells. Science 296, 913–916.

Žárský V, Cvrčková F, Potocký M, Hála M (2009). Exocytosis and cell polarity in plants— exocyst and recycling domains. New Phytol 183, 255–272.

Zhang X, Bi E, Novick P, Du L, Kozminski KG, Lipschutz JH, Guo W (2001). Cdc42 interacts with the exocyst and regulates polarized secretion. J Biol Chem 276, 46745–46750.

Zhang X, Orlando K, He B, Xi F, Zhang J, Zajac A, Guo W (2008). Membrane association and functional regulation of Sec3 by phospholipids and Cdc42. J Cell Biol 180, 145–158.